Inorg. Chem. **2005**, *44*, 6949–6958

Magnetism of Cyano-Bridged Ln^{3+}–M^{3+} Complexes. Part II: One-Dimensional Complexes (Ln^{3+} = Eu, Tb, Dy, Ho, Er, Tm; M^{3+} = Fe or Co) with bpy as Blocking Ligand

Albert Figuerola,[†] Joan Ribas,[†] David Casanova,[†] Miguel Maestro,[‡] Santiago Alvarez,*[,†] and Carmen Diaz*[,†]

Departament de Química Inorgànica, Universitat de Barcelona, Martí i Franquès, 1-11, 08028 Barcelona, and Departamento de Química Fundamental, Facultade de Ciencias, Universidade da Coruña,15071 A Coruña, Spain

Received April 27, 2005

The reaction of $Ln(NO_3)_{3(aq)}$ with $K_3[Fe(CN)_6]$ or $K_3[Co(CN)_6]$ and 2,2′-bipyridine in water/ethanol led to 13 one-dimensional complexes: *trans*-$[M(CN)_4(\mu\text{-}CN)_2Ln(H_2O)_4(bpy)]_n \cdot 4nH_2O \cdot 1.5n$bpy ($Ln = Eu^{3+}$, Tb^{3+}, Dy^{3+}, Ho^{3+}, Er^{3+}, Tm^{3+}, Lu^{3+}; $M = Fe^{3+}$, Co^{3+}). The structures for $[EuFe]_n$ (**1**), $[TbFe]_n$ (**2**), $[DyFe]_n$ (**3**), $[HoFe]_n$ (**4**), $[ErFe]_n$ (**5**), $[TmFe]_n$ (**6**), $[LuFe]_n$ (**7**), $[EuCo]_n$ (**8**), $[TbCo]_n$ (**9**), $[DyCo]_n$ (**10**), $[HoCo]_n$ (**11**), $[ErCo]_n$ (**12**), and $[TmCo]_n$ (**13**) have been solved: they crystallize in the triclinic space group $P\bar{1}$ and are isomorphous. They exhibit a supramolecular architecture created by the interplay of coordinative, hydrogen bonding, and π–π interactions. A stereochemical study of the eight-vertex polyhedra of the lanthanide ions, based on continuous shape measures, is presented. The Ln^{3+}–Fe^{3+} interaction is antiferromagnetic in $[DyFe]_n$ and $[TbFe]_n$. For $[EuFe]_n$, $[HoFe]_n$, $[ErFe]_n$, and $[TmFe]_n$, there is no sign of any significant interaction. The magnetic behavior of $[DyFe]_n$ suggests the onset of weak long-range ferromagnetic ordering at 2.5 K.

Introduction

Paramagnetic lanthanide ions are attracting much interest in the field of molecule-based magnetic materials due to their large anisotropic magnetic moments.[1] Indeed, hybrid dimetallic cyano-bridged Prussian Blue analogues giving one- to three-dimensional coordination polymers based on $[M(CN)_6]^{3-}$ (M = Fe, Cr, Mn) have attracted great attention because of their rich structures and magnetic behavior.[2] These studies were mainly focused on transition metals. In principle, it would be possible to enhance the coercive field by introducing paramagnetic lanthanide ions because these possess rather large and anisotropic moments. To date, magnetic studies have been made for several cyano-bridged lanthanide–transition metal complexes with different dimensionality: dinuclear,[3] trinuclear,[4] tetranuclear,[5] one-dimensional,[4a,6] two-dimensional,[6e,7] and three-dimensional.[8] In most cases, the magnetic properties of these complexes do not seem exciting,

* To whom correspondence should be addressed. E-mail: carme.diaz@qi.ub.es.
[†] Universitat de Barcelona
[‡] Universidade da Coruña

(1) (a) Benelli, C.; Gatteschi, D. *Chem. Rev.* **2002**, *102*, 2369. (b) de Sá, G. F.; Malta, O. P.; de Mello Donegá, C.; Simas, A. M.; Longo, R. L.; Santacruz, P. A.; da Silva, E. F., Jr. *Coord. Chem. Rev.* **2000**, *196*, 165.
(2) (a) Ohba, M.; Õkawa, H. *Coord. Chem. Rev.* **2000**, *198*, 313. (b) Verdaguer, M.; Bleuzen, A.; Marvaud, V.; Vaissermann, J.; Seuleiman, M.; Desplanches, C.; Scuiller, A.; Train, C.; Garde, R.; Gelly, G.; Lomenech, C.; Rosenman, I.; Veillet, P.; Cartier, C.; Villain, F. *Coord. Chem. Rev.* **1999**, *190*−*192*, 1023.
(3) (a) Gao G.; Ma, B.; Wang, Z.; Yi, T.; Liao, C.; Yan, C.; Xu, G. *Mol. Cryst. Liq. Cryst.* **1999**, *335*, 201. (b) Figuerola, A.; Diaz, C., Ribas, J.; Tangoulis, V.; Granell, J.; Lloret, F.; Mahía, J.; Maestro, M. *Inorg. Chem.* **2003**, 641. (c) Sun, X. R.; Chen, Z. D.; Yan, F.; Gao, S.; Cheung, K. K.; Che, C. M.; Zhang, X. X. *J. Cluster Sci.* **2002**, *13*, 103.
(4) (a) Yan, B.; Chen, Z. *Helv. Chim. Acta* **2001**, *84*, 817. (b) *Chem. Lett.* **2000**, *11*, 1244. (b) Yi, T.; Gao, S.; Chen, X. W.; Yan, C. H.; Li, B. G. *Acta Crystallogr.* **1998**, *C54*, 41.
(5) (a) Kou, H. Z.; Gao, S.; Li, C. H.; Liao, D. Z.; Zhou, B. C.; Wang, R. J.; Li, Y. *Inorg. Chem.* **2002**, *41*, 4756. (b) Gao, S.; Ma, B. Q.; Sun, H. L. Li, J. R. *J. Solid State Chem.* **2003**, *171*, 201.
(6) (a) Figuerola, A.; Diaz, C.; Ribas, J.; Vassilis, T.; Sangregorio, C.; Gatteschi, D.; Maestro, M.; Mahía, J. *Inorg. Chem.* **2003**, *42*, 5274. (b) Figuerola, A.; Diaz, C.; El Falah, M. S.; Ribas, J.; Maestro, M.; Mahía, J. *Chem. Commun.* **2001**, 1204. (b) Yan, B.; Wang, H. D.; Chen, Z. D. *Polyhedron* **2001**, *20*, 591. (c) Yan, B.; Chen, Z.; Wang, S.; Gao, S. *Chem Lett.* **2001**, 350. (d) Kou, H. Z.; Gao, S.; Jin, X. *Inorg. Chem.* **2001**, *40*, 6295.
(7) (a) Kou, H. Z.; Gao, S.; Sun, B. W.; Zhang, J. *Chem. Mater* **2001**, *13*, 1433. (c) Zhao, Q. H.; Wang, Q. H.; Fang, R. B. *Trans. Met. Chem.* **2004**, *29*, 144. (d) Ma, B. Q.; Gao, S.; Su, G.; Xu, G. X. *Angew. Chem., Int. Ed.* **2001**, *40*, 434.
(8) Hulliger, F.; Landolt, M.; Vetsch, H. *J. Solid State Chem.* **1976**, *18*, 283.

10.1021/ic050650+ CCC: $30.25
Published on Web 08/31/2005

since the coupling between the lanthanide and transition metals is very weak because of the effective shielding of the 4f electrons by the outer-shell electrons. Important magnetic properties were found in only a few cyano-bridged rare earth−transition metal complexes. The 3D polymer $[SmFe(CN)_6]\cdot 4H_2O$, with strong anisotropic coercive field, exhibits a long-range ferrimagnetic ordering below 3.5 K, and the analogous $[TbCr(CN)_6]\cdot 4H_2O$ has the highest magnetic-phase transition temperature of 11.7 K for lanthanide−iron−cyanide systems.[8] The 2D polymer $[Gd(DMF)_2(H_2O)_2Cr(CN)_6]\cdot H_2O$ (DMF = *N*,*N*′-dimethylformamide) has a long-range antiferromagnetic ordering below 3.5 K,[7a] and the analogous $[Sm(DMF)_2(H_2O)_2Cr(CN)_6]\cdot H_2O$ shows a long-range ferromagnetic ordering below 4.2 K.[6e] The 1D polymer $[Sm(DMA)_2(H_2O)_4Fe(CN)_6]\cdot 5H_2O$ (DMA = *N*,*N*′-dimethylacetamide) has a long-range magnetic ordering below 3.5 K,[4a] the $[Sm(DMF)_4(H_2O)_2Mn(CN)_6]\cdot H_2O$ has a long-range magnetic ordering at 18 K,[6d] and the $[Fe(CN)_4(\mu\text{-}CN)_2Sm(H_2O)_4(bpy)]_n\cdot 5nH_2O\cdot 1{,}5n$bpy (bpy = 2,2′-bipyridine) 1D complex, previously reported by us, has a long-range magnetic ordering at 3.5 K.[6a] No long-range magnetic ordering was found in systems of lower dimensionality. This implies that increasing the number of dimensions may enhance and improve bulk magnetic properties. Part II of this work is focused on the study of the magnetic behavior of the new chains of formula: *trans*-$[Fe(CN)_4(\mu\text{-}CN)_2Eu(H_2O)_4(bpy)]_n\cdot 4nH_2O\cdot 1.5n$bpy (**1**), *trans*-$[Fe(CN)_4(\mu\text{-}CN)_2Tb(H_2O)_4(bpy)]_n\cdot 4nH_2O\cdot 1.5n$bpy (**2**), *trans*-$[Fe(CN)_4(\mu\text{-}CN)_2Dy(H_2O)_4(bpy)]_n\cdot 4nH_2O\cdot 1.5n$bpy (**3**), *trans*-$[Fe(CN)_4(\mu\text{-}CN)_2Ho(H_2O)_4(bpy)]_n\cdot 4nH_2O\cdot 1.5n$bpy (**4**), *trans*-$[Fe(CN)_4(\mu\text{-}CN)_2Er(H_2O)_4(bpy)]_n\cdot 4nH_2O\cdot 1.5n$bpy (**5**), *trans*-$[Fe(CN)_4(\mu\text{-}CN)_2Tm(H_2O)_4(bpy)]_n\cdot 4nH_2O\cdot 1.5n$bpy (**6**), *trans*-$[Fe(CN)_4(\mu\text{-}CN)_2Lu(H_2O)_4(bpy)]_n\cdot 4nH_2O\cdot 1.5n$bpy (**7**), *trans*-$[Co(CN)_4(\mu\text{-}CN)_2Eu(H_2O)_4(bpy)]_n\cdot 4nH_2O\cdot 1.5n$bpy (**8**), *trans*-$[Co(CN)_4(\mu\text{-}CN)_2Tb(H_2O)_4(bpy)]_n\cdot 4nH_2O\cdot 1.5n$bpy (**9**), *trans*-$[Co(CN)_4(\mu\text{-}CN)_2Dy(H_2O)_4(bpy)]_n\cdot 4nH_2O\cdot 1.5n$bpy (**10**), *trans*-$[Co(CN)_4(\mu\text{-}CN)_2Ho(H_2O)_4(bpy)]_n\cdot 4nH_2O\cdot 1.5n$bpy (**11**), *trans*-$[Co(CN)_4(\mu\text{-}CN)_2Er(H_2O)_4(bpy)]_n\cdot 4nH_2O\cdot 1.5n$bpy (**12**), and *trans*-$[Co(CN)_4(\mu\text{-}CN)_2Tm(H_2O)_4(bpy)]_n\cdot 4nH_2O\cdot 1.5n$bpy (**13**), all of which are isostructural and with the *trans*-$[M(CN)_4(\mu\text{-}CN)_2Ln(H_2O)_4(bpy)]_n\cdot 4nH_2O\cdot 1.5n$bpy ($M^{3+}$ = Fe or Co; Ln^{3+}= Sm^{3+}, Gd^{3+} or Yb^{3+}) previously reported by us.[6a]

Experimental Section

Materials All starting materials were purchased from Aldrich and were used without further purification.

Synthesis of the New Complexes. *trans*-$[Fe(CN)_4(\mu\text{-}CN)_2Eu(H_2O)_4(bpy)]_n\cdot 4nH_2O\cdot 1.5n$bpy (1), *trans*-$[Fe(CN)_4(\mu\text{-}CN)_2Tb(H_2O)_4(bpy)]_n\cdot 4nH_2O\cdot 1.5n$bpy (2), *trans*-$[Fe(CN)_4(\mu\text{-}CN)_2Dy(H_2O)_4(bpy)]_n\cdot 4nH_2O\cdot 1.5n$bpy (3), *trans*-$[Fe(CN)_4(\mu\text{-}CN)_2Ho(H_2O)_4(bpy)]_n\cdot 4nH_2O\cdot 1.5n$bpy (4), *trans*-$[Fe(CN)_4(\mu\text{-}CN)_2Er(H_2O)_4(bpy)]_n\cdot 4nH_2O\cdot 1.5n$bpy (5), *trans*-$[Fe(CN)_4(\mu\text{-}CN)_2Tm(H_2O)_4(bpy)]_n\cdot 4nH_2O\cdot 1.5n$bpy (6), and *trans*-$[Fe(CN)_4(\mu\text{-}CN)_2Lu(H_2O)_4(bpy)]_n\cdot 4nH_2O\cdot 1.5n$bpy (7). The seven $[Fe-Ln]_n$ complexes were obtained by adding a solution of $Ln(NO_3)_3.nH_2O$ (n = 5, 6) (2.2 mmol) in water (15 mL) to an equimolar solution of $K_3[Fe(CN)_6]$ in water (50 mL). To this mixture an ethanolic solution (10 mL) of 2,2′-bipyridine (3.3 mmol) was added. The solution was left undisturbed, and well-formed orange crystals were obtained for all of them after several days (yields ca. 80%). Anal. Calcd for **1**, $C_{31}H_{36}EuFeN_{11}O_8$: C, 41.44; N, 17.15; H, 4.04. Found: C, 41.5; N, 17.2; H, 4.02. Anal. Calcd for **2**, $C_{31}H_{36}FeN_{11}O_8Tb$: C, 41.12; N, 17.02; H, 4.00. Found: C, 41.0; N, 17.2; H, 3.9. Anal. Calcd for **3**, $C_{31}H_{36}DyFeN_{11}O_8$: C, 40.96; N, 16.95; H, 3.99. Found: C, 41.1; N, 17.0; H, 3.9. Anal. Calcd for **4**, $C_{31}H_{36}FeHoN_{11}O_8$: C, 40.85; N, 16.90; H, 3.98. Found: C, 40.9; N, 17.1; H, 4.1. Anal. Calcd for **5**, $C_{31}H_{36}ErFeN_{11}O_8$: C, 40.74; N, 16.86; H, 3.97. Found: C, 40.8; N, 17.2; H, 3.9. Anal. Calcd for **6**, $C_{31}H_{36}FeN_{11}O_8Tm$: C, 40.67; N, 16.83; H, 3.96. Found: C, 40.6; N, 16.8; H, 3.9. Anal. Calcd for **7**, $C_{31}H_{36}FeLuN_{11}O_8$: C, 40.40; N, 16.72; H, 3.94. Found: C, 40.2; N, 16.6; H, 3.8.

***trans*-$[Co(CN)_4(\mu\text{-}CN)_2Eu(H_2O)_4(bpy)]_n\cdot 4nH_2O\cdot 1.5n$bpy (8), *trans*-$[Co(CN)_4(\mu\text{-}CN)_2Tb(H_2O)_4(bpy)]_n\cdot 4nH_2O\cdot 1.5n$bpy (9), *trans*-$[Co(CN)_4(\mu\text{-}CN)_2Dy(H_2O)_4(bpy)]_n\cdot 4nH_2O\cdot 1.5n$bpy (10), *trans*-$[Co(CN)_4(\mu\text{-}CN)_2Ho(H_2O)_4(bpy)]_n\cdot 4nH_2O\cdot 1.5n$bpy (11), *trans*-$[Co(CN)_4(\mu\text{-}CN)_2Er(H_2O)_4(bpy)]_n\cdot 4nH_2O\cdot 1.5n$bpy (12), and *trans*-$[Co(CN)_4(\mu\text{-}CN)_2Tm(H_2O)_4(bpy)]_n\cdot 4nH_2O\cdot 1.5n$bpy (13).** The six complexes were obtained by the same procedure using $K_3[Co(CN)_6]$ instead of $K_3[Fe(CN)_6]$. Well-formed colorless crystals were obtained after several days (yields ca. 80%). Anal. Calcd for **8**, $C_{31}H_{36}CoEuN_{11}O_8$: C, 41.30; N, 17.09; H, 4.02. Found: C, 41.2; N, 17.0; H, 4.2. Anal. Calcd for **9**, $C_{31}H_{36}CoN_{11}O_8Tb$: C, 40.98; N, 16.95; H, 3.99. Found: C, 41.0; N, 17.0; H, 3.9. Anal. Calcd for **10**, $C_{31}H_{36}CoDyN_{11}O_8$: C, 40.82; N, 16.90; H, 3.98. Found: C, 40.9; N,17.0; H 4.1. Anal. Calcd for **11**, $C_{31}H_{36}CoHoN_{11}O_8$: C, 40.71; N, 16.85; H, 3.96. Found: C, 40.8; N, 16.9; H, 4.1. Anal. Calcd for **12**, $C_{31}H_{36}CoErN_{11}O_8$: C, 40.60; N, 16.80; H, 3.96. Found: C, 40.7; N, 16.7; H, 4.0. Anal. Calcd for **13**, $C_{31}H_{36}CoN_{11}O_8Tm$: C, 40.53; N, 16.77; H, 3.95. Found: C, 40.6; N, 16.7; H, 3.9.

Crystal Structure Determination. The crystal data and details on the data collection and refinement are summarized in Tables 1 and 2 for complexes **1**−**6** and **8**−**13**, respectively, and Table S1 for complex **7** (Supporting Information). The crystal data for complexes **1**−**13** were collected using a Bruker SMART CCD-based diffractometer operating at room temperature, except for that for **5**, which were recorded at 173(2) K. Intensities were collected with graphite monochromatized Mo Kα radiation (λ = 0.71073 Å) operating at 50 kV and 30 mA, using the $\omega/2\theta$ scan technique. Suitable single crystals were obtained at room temperature by slow evaporation of solutions of the complexes. A total of 1271 frames of intensity data were collected over a hemisphere of the reciprocal space by combination of three exposure sets. Each frame covered 0.3° in ω, and the first 50 frames were recollected at the end of data collection to monitor crystal decay (Tables 1, 2 and S1). The refinement method employed was full-matrix least-squares on F^2. The results of the integration process are summarized in Tables 1, 2, and S1. Absorption corrections were applied using the SADABS program[9] (the maximum and minimum transmission coefficients are in Tables 1, 2, and S1). The structures were solved using the Bruker SHELXTL-PC software[10] by direct methods and refined by full-matrix least-squares methods on F^2. All non-hydrogen atoms were refined anisotropically, except in the case of crystallization solvents with high thermal disorder. Hydrogen atoms were included in calculated positions and refined in the riding mode, except those

(9) Sheldrick, G. M. *SADABS, A Program for Empirical Absorption Correction of Area Detector Data*; University of Göttingen: Göttingen, Germany, 1996. Based on the method of Robert Blessing: Blessing, R. H. *Acta Crystallogr*. **1995**, *A51*, 33.

(10) Sheldrick, G. M. *SHELXS-97, A Program for Solving Crystal Structures and Crystal Structure Refinement*; University of Göttingen: Göttingen, Germany, 1997.

Table 1. Crystal Parameters for **1**−**6**

	$[EuFe]_n$ (**1**)	$[TbFe]_n$ (**2**)	$[DyFe]_n$ (**3**)	$[HoFe]_n$ (**4**)	$[ErFe]_n$ (**5**)	$[TmFe]_n$ (**6**)
empirical formula	$C_{62}H_{72}N_{22}O_{16}Fe_2Eu_2$	$C_{62}H_{72}N_{22}O_{16}Fe_2Tb_2$	$C_{62}H_{72}N_{22}O_{16}Fe_2Dy_2$	$C_{62}H_{72}N_{22}O_{16}Fe_2Ho_2$	$C_{62}H_{72}N_{22}O_{16}Fe_2Er_2$	$C_{62}H_{72}N_{22}O_{16}Fe_2Tm_2$
fw	1797.04	1810.96	1818.12	1822.98	1827.64	1830.98
cryst size (mm^3)	0.50 × 0.36 × 0.12	0.33 × 0.20 × 0.20	0.38 × 0.30 × 0.22	0.50 × 0.21 × 0.07	0.50 × 0.17 × 0.06	0.41 × 0.21 × 0.13
cryst habit, color	prism, orange	prism, orange	prism, orange	prism, orange	needle, orange	prism, orange
cryst syst	triclinic	triclinic	triclinic	triclinic	triclinic	triclinic
space group	$P\bar{1}$	$P\bar{1}$	$P\bar{1}$	$P\bar{1}$	$P\bar{1}$	$P\bar{1}$
Z	1	1	1	1	1	1
a (Å)	9.7631(4)	9.7458(5)	9.7403(8)	9.7430(4)	9.7267(6)	9.7316(7)
b (Å)	10.6766(4)	10.6465(5)	10.6329(8)	10.6165(4)	10.5917(6)	10.5930(7)
c (Å)	19.9719(8)	19.9583(10)	19.9447(16)	19.9746(8)	19.7480(12)	19.9733(13)
α (deg)	83.047(1)	83.165(1)	83.286(1)	83.294(1)	83.205(1)	83.356(1)
β (deg)	83.902(1)	84.099(1)	84.284(1)	84.400(1)	84.222(1)	84.571(1)
γ (deg)	64.314(1)	64.131(1)	63.994(1)	63.983(1)	63.997(1)	63.808(1)
V ($Å^3$)	1858.93(13)	1847.09(16)	1841.0(3)	1841.54(13)	1812.98(19)	1833.0(2)
ρ (calcd) (g/cm^3)	1.605	1.628	1.640	1.644	1.674	1.659
μ_{calc} (mm^{-1})	2.124	2.354	2.471	2.590	2.763	2.864
T (K)	298(2)	298(2)	298(2)	298(2)	173(2)	298(2)
F(000)	904	908	910	912	914	916
transmission factors (max; min)	0.7846; 0.4164	0.6503; 0.5104	0.6125; 0.4536	0.8395; 0.3576	0.8518; 0.3388	0.7072; 0.2807
decay (%)	1.0	0	0	0	0	0
scan type	ϕ and ω	ϕ and ω	ϕ and ω	ϕ and ω	ϕ and ω	ϕ and ω
Θ range for data collection	2.06−28.27°	2.06−28.28°	2.06−28.28°	2.06−28.29°	2.05−26.37°	2.06−28.25°
total reflns	12 047	11 992	11 964	11 831	11 302	11 873
independent reflns [R(int)]	8451 [0.0182]	8402 [0.0168]	8387 [0.0166]	8350 [0.0229]	7346 [0.0303]	8329 [0.0159]
completeness to Θ_{max}	91.7%	91.7%	91.8%	91.4%	98.9	91.9%
absorption correction	multiscan	multiscan	multiscan	multiscan	multiscan	multiscan
parameters refined, restraints	505, 0	505, 0	516, 0	522, 0	508, 0	489, 0
final R indices[a] [$I > 2\sigma(I)$]	0.0275	0.0253	0.0239	0.0270	0.0328	0.0219
final wR2 indices (all data)[a]	0.0717	0.0667	0.0616	0.0709	0.1103	0.0534
weights[b] (a, b)	0.0387, 0.9857	0.0369, 1.0444	0.0329, 0.6402	0.0411, 0.1208	0.0695, 0	0.0258, 0.2807
GOF on F^2	1.043	1.020	1.020	1.044	1.126	1.045
largest diff. peak and hole ($eÅ^{-3}$)	0.967 and −0.993	0.865 and −0.918	0.623 and −0.630	1.357 and −1.752	1.070 and −1.227	0.653 and −0.705

[a] $R1 = \sum||F_0| - |F_c||$ and $wR2 = \{\sum[w(F_0^2 - F_c^2)]/\sum[w(F_0^2)^2]\}^{1/2}$. [b] The weighting scheme employed was $w = [\sigma^2(F_0^2 + (aP)^2 + bP]]$ and $P = (|F_0|^2+2|F_c|^2)/3$.

of water molecules, which were located on residual density maps, but then their positions were fixed and refined in the riding mode. The low completeness to Θ_{max} (83,8%) for **7** (Table S1, Supporting Information) was due to a diffractometer problem. We can conclude, from the results of the study of their crystal structure, that it is isostructural with complexes **1**−**6** and **8**−**13**, so we do not repeat their data collection.

Physical Measurements. Magnetic measurements were carried out in the "Servei de Magnetoquímica (Universitat de Barcelona)" on polycrystalline samples (20 mg) with a Quantum Design SQUID MPMS-XL magnetometer working in the 2−300 K range. The magnetic field was 8000 G. The field-dependent magnetization was measured in the applied magnetic field range 0−5 T. The diamagnetic corrections were evaluated from Pascal's constants.

Results and Discussion

Description of the Structures of Complexes 1−6 and 8−13. In all cases, the crystal system is triclinic and the space group is $P\bar{1}$. Their crystallographic analysis revealed that they all confine isomorphous one-dimensional polymers, as shown in Figure 1. An ORTEP view of the $[Dy-Fe]_n$ (**3**) complex with the atom-labeling scheme is represented, as an example, in Figure 1a. Selected bond lengths and angles for **1**−**6** and **8**−**13** are listed in Tables 3 and 4, respectively; those for complex **7** are listed in Table S2 (Supporting Information). The data for **7** (not shown by low Θ_{max} completeness) agree with those observed for the rest of compounds. The chain is made by the cyano-bridged alternating $M(CN)_6-Ln(H_2O)_4$-(bpy) (M= Fe^{3+}, Co^{3+}) fragment. The Ln^{3+} ions are eight-coordinated with four oxygen atoms of four water molecules, two nitrogen atoms of the 2,2′-bipyridine ligand, and two nitrogen atoms of the cyanide bridges. The longest Ln−O and Ln−N distances correspond to the Eu^{3+} ion and the shortest ones to the Tm^{3+} ion in accordance with the variation of the radius of the lanthanide ions. Six cyanide ligands surround the M^{3+} ion in a distorted octahedral environment. The lowest M−C distances correspond as expected to the $[Co(CN)_6]^{3-}$. Each $[M(CN)_6]$ (M^{3+} = Fe, Co) coordinates to two Ln^{3+} ions using two trans cyanide ligands, while each $Ln(H_2O)_4$(bpy) group connects two $[M(CN)_6]$ moieties in a cis fashion, yielding a chain; a schematic view of the chain of $[NdFe]_n$ is shown, as an example, in Figure 1b. The angles Ln−M−Ln and M−Ln−M have the same value in each compound (159.58° for **1**, 159.49° for **2**, 159.44° for **3**, 159.41° for **4**, 159.424° for **5**, 159.34° for **6**, 159.59° for **8**, 159.52° for **9**, 159.48° for **10**, 159.44° for **11**, 159.41° for **12**, and 159.40° for **13**), so the chain runs along the structure in a perfect zigzag path. Each lanthanide ion has two different intramolecular distances with each of the two neighboring M ions, so the chain could be considered as an alternating

Table 2. Crystal Parameters for **8**−**13**

	$[EuCo]_n$ (**8**)	$[TbCo]_n$ (**9**)	$[DyCo]_n$ (**10**)	$[HoCo]_n$ (**11**)	$[ErCo]_n$ (**12**)	$[TmCo]_n$ (**13**)
empirical formula	$C_{62}H_{72}N_{22}O_{16}Co_2Eu_2$	$C_{62}H_{72}N_{22}O_{16}Co_2Tb_2$	$C_{62}H_{72}N_{22}O_{16}Co_2Dy_2$	$C_{62}H_{72}N_{22}O_{16}Co_2Ho_2$	$C_{62}H_{72}N_{22}O_{16}Co_2Er_2$	$C_{62}H_{72}N_{22}O_{16}Co_2Tm_2$
fw	1803.20	1817.12	1824.28	1833.17	1869.83	1837.14
cryst size (mm^3)	0.50 × 0.21 × 0.16	0.50 × 0.25 × 0.25	0.50 × 0.28 × 0.25	0.37 × 0.16 × 0.14	0.50 × 0.38 × 0.12	0.50 × 0.31 × 0.13
cryst habit, color	prism, colorless	prism, colorless	prism, colorless	prism, colorless	prism, colorless	prism, colorless
cryst syst	triclinic	triclinic	triclinic	triclinic	triclinic	triclinic
space group	$P\bar{1}$	$P\bar{1}$	$P\bar{1}$	$P\bar{1}$	$P\bar{1}$	$P\bar{1}$
Z	1	1	1	1	1	1
a (Å)	9.7263(6)	9.7128(11)	9.7016(4)	9.6954(4)	9.6897(4)	9.6883(5)
b (Å)	10.6415(7)	10.5886(12)	10.5779(5)	10.5647(4)	10.5492(5)	10.5465(5)
c (Å)	20.0284(13)	20.017(2)	20.0008(9)	20.0042(7)	20.0209(9)	20.0435(10)
α (deg)	83.022(1)	83.262(2)	83.254(1)	83.317(1)	83.355(1)	83.388(1)
β (deg)	84.001(1)	84.258(2)	84.352(1)	84.451(1)	84.575(1)	84.632(1)
γ (deg)	64.217(1)	64.088(2)	63.971(1)	63.875(1)	63.802(1)	63.789(1)
V ($Å^3$)	1849.7(2)	1836.1(4)	1829.05(14)	1824.52(12)	1821.77(14)	1823.09(16)
ρ (calcd) (g/cm^3)	1.619	1.643	1.654	1.688	1.704	1.673
μ_{calc} (mm^{-1})	2.191	2.425	2.544	2.671	2.810	2.936
T (K)	298(2)	298(2)	298(2)	298(2)	298(2)	298(2)
F(000)	906	910	910	918	936	918
transmission factors (max; min)	0.7206; 0.4071	0.5823; 0.3768	0.5688; 0.3628	0.7062; 0.4382	0.7291; 0.3339	0.7014; 0.3215
decay (%)	0	0	0	0.3	0	0.1
scan type	ϕ and ω	ϕ and ω	ϕ and ω	ϕ and ω	ϕ and ω	ϕ and ω
Θ range for data collection	2.05−28.24°	2.05−28.27°	2.05−28.27°	2.05−28.29°	2.05−28.29°	2.16−28.26°
total reflns	11 940	11 587	11 813	11 925	11 644	11 761
independent reflns [R(int)]	8377 [0.0192]	8265 [0.0171]	8287 [0.0154]	8327 [0.0181]	8242 [0.0260]	8256 [0.0160]
completeness to Θ_{max}	91.7%	90.9%	91.5%	92.0%	91.1	91.5%
absorption correction	multiscan	multiscan	multiscan	multiscan	multiscan	multiscan
parameters refined, restraints	490, 0	491, 0	488, 0	486, 0	488, 0	469, 0
final R indices[a] [$I > 2\sigma(I)$]	0.0267	0.0281	0.0218	0.0262	0.0331	0.0236
final wR2 indices (all data)[a]	0.0666	0.0907	0.0552	0.0650	0.0897	0.0599
weights[b] (a, b)	0.0369, 0	0.0619, 0.5745	0.0285, 0.5321	0.0343, 0.6764	0.0528, 1.55434	0.0328, 0.5933
GOF on F^2	1.016	1.091	1.034	1.000	1.034	1.048
largest diff. peak and hole ($eÅ^{-3}$)	0.638 and −0.896	1.646 and −1.842	0.865 and −0.954	0.732 and −0.786	1.376 and −2.424	0.994 and −1.085

[a] $R1 = \sum||F_0| - |F_c||$ and $wR2 = \{\sum[w(F_0^2 - F_c^2)]/\sum[w(F_0^2)^2]\}^{1/2}$. [b] The weighting scheme employed was $w = [\sigma^2(F_0^2 + (aP)2$.

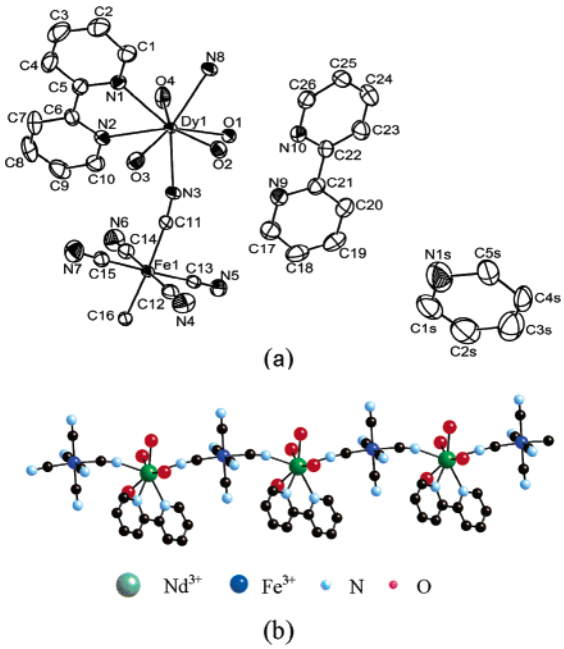

Figure 1. (a) ORTEP view of complex *trans*-$[Fe(CN)_4(\mu\text{-}CN)_2Dy(H_2O)_4(bpy)]_n \cdot 4nH_2O.1.5nbpy$ (**3**) with atom labeling scheme (ellipsoids drawn at 50% probability level). All complexes are isostructural. (b) Schematic representation of the chain of [NdFe].

chain (5.489 and 5.593 Å for **1**, 5.464 and 5.565 Å for **2**, 5.448 and 5.550 Å for **3**, 5.444 and 5.544 Å for **4**, 5.435 and 5.537 Å for **5**, 5.421 and 5.523 Å for **6**, 5.461 and 5.567 Å for **8**, 5.436 and 5.536 Å for **9**, 5.421 and 5.522 Å for **10**, 5.407 and 5.509 Å for **11**, 5.396 and 5.499 Å for **12**, and 5.395 and 5.496 Å for **13**). Between the chains, there are water and bipyridine crystallization molecules. It is interesting to note that the bpy of crystallization adopts two different stereo configurations. One of them is not planar, showing a dihedral angle (N−C−C−N) of 16.8° for **1**, 17.0° for **2**, 16.7° for **3**, 16.8° for **4**, 16.7° for **5**, 16.6° for **6**, 17.4° for **8**, 17.5° for **9**, 17.2° for **10**, 17.7° for **11**, 17.1° for **12**, and 16.6° for **13**; the other configuration is planar, and the same dihedral angle is 180°. Bond lengths and angles of the bpy ligand are similar to those observed in the free bpy molecules, taking into account the abnormal trans configuration. A supramolecular 3D network is given by hydrogen bonds involving the nitrogen atoms of the bpy of crystallization, the four oxygen atoms of the H_2O ligands of the $Ln(H_2O)_4$-(bpy) entity, the nitrogen atom of two of the four terminal CN^- ligands of the $[M(CN)_6]$ entity, and the water molecules of crystallization (Table S3, Supporting Information). The trans-bpy of crystallization and the bpy ligands of two neighboring chains exhibit a weak $\pi-\pi$ interaction (Figure 2); these interactions justify that the bpy ligands are situated along the chain in the cis position. A $\pi-\pi$ interaction between each of neighboring nonplanar bpy of crystallization is also present in the crystal. This interaction, together with

Table 3. Selected Bonds Lengths (Å) and Angles (deg) for **1**−**6**

	[Eu−Fe]$_n$ (**1**)	[Tb−Fe]$_n$ (**2**)	[Dy−Fe]$_n$ (**3**)	[Ho−Fe]$_n$ (**4**)	[Er−Fe]$_n$ (**5**)	[Tm−Fe]$_n$ (**6**)
Ln(1)−O(1)	2.397(2)	2.398(2)	2.360(2)	2.350(2)	2.347(3)	2.347(2)
Ln(1)−O(2)	2.427(2)	2.372(2)	2.381(2)	2.374(2)	2.368(4)	2.329(2)
Ln(1)−O(3)	2.434(2)	2.343(3)	2.405(2)	2.391(2)	2.378(3)	2.296 (2)
Ln(1)−O(4)	2.385(2)	2.413(2)	2.332(2)	2.323(2)	2.312(4)	2.373(2)
Ln(1)−N(1)	2.555(2)	2.564(2)	2.515(2)	2.505(2)	2.525(4)	2.482(2)
Ln(1)−N(2)	2.589(2)	2.528(2)	2.547(2)	2.541(2)	2.489(4)	2.525(2)
Ln(1)−N(3)	2.495(2)	2.478(2)	2.445(2)	2.436(2)	2.440(4)	2.410(2)
Ln(1)−N(8)	2.509(2)	2.462(2)	2.467(2)	2.455(2)	2.418(4)	2.434(2)
Fe(1)−C(11)	1.937(3)	1.944(3)	1.937(2)	1.935(3)	1.945(5)	1.940(2)
Fe(1)−C(12)	1.954(3)	1.948(3)	1.950(3)	1.958(3)	1.948(5)	1.953(3)
Fe(1)−C(13)	1.956(3)	1.954(3)	1.958(3)	1.951(3)	1.950(5)	1.957(3)
Fe(1)−C(14)	1.944(3)	1.954(3)	1.950(3)	1.943(3)	1.943(6)	1.955(3)
Fe(1)−C(15)	1.937(3)	1.938(3)	1.941(3)	1.954(3)	1.938(6)	1.936(3)
Fe(1)−C(16)	1.947(3)	1.932(3)	1.945(2)	1.950(3)	1.934(5)	1.949(2)
N(3)−C(11)	1.145(4)	1.154(3)	1.148(3)	1.152(4)	1.163(7)	1.148(3)
C(11)−N(3)−Ln(1)	164.1(2)	175.4(2)	165.0(2)	165.6(2)	175.9(4)	165.9(2)
N(3)−C(11)−Fe(1)	173.5(2)	175.8(2)	172.8(2)	172.7(2)	175.4(4)	172.5(2)

Table 4. Selected Bonds Lengths (Å) and Angles (deg) for **8**−**13**

	[Eu−Co]$_n$ (**8**)	[Tb−Co]$_n$ (**9**)	[Dy−Co]$_n$ (**10**)	[Ho−Co]$_n$ (**11**)	[Er−Co]$_n$ (**12**)	[Tm−Co]$_n$ (**13**)
Ln(1)−O(1)	2.379(2)	2.420(2)	2.4065(17)	2.316(2)	2.339(2)	2.3478(19)
Ln(1)−O(2)	2.3922(19)	2.392(2)	2.3810(17)	2.343(2)	2.359(3)	2.3266(18)
Ln(1)−O(3)	2.4244(19)	2.370(2)	2.3563(16)	2.374(2)	2.308(3)	2.299(2)
Ln(1)−O(4)	2.4503(19)	2.348(3)	2.3360(18)	2.394(2)	2.390(3)	2.3757(19)
Ln(1)−N(1)	2.550(2)	2.558(3)	2.5117(19)	2.536(2)	2.488(3)	2.517(2)
Ln(1)−N(2)	2.590(2)	2.524(3)	2.5490(19)	2.501(2)	2.531(3)	2.477(2)
Ln(1)−N(3)	2.505(2)	2.493(3)	2.4541(19)	2.465(2)	2.429(3)	2.446(2)
Ln(1)−N(8)	2.521(2)	2.465(3)	2.4805(19)	2.442(2)	2.455(3)	2.421(2)
Co(1)−C(11)	1.903(2)	1.904(3)	1.897(2)	1.909(3)	1.901(3)	1.909(2)
Co(1)−C(12)	1.910(3)	1.911(3)	1.904(3)	1.910(3)	1.905(4)	1.905(3)
Co(1)−C(13)	1.915(3)	1.905(4)	1.910(2)	1.909(3)	1.913(4)	1.899(3)
Co(1)−C(14)	1.902(3)	1.896(3)	1.904(3)	1.899(3)	1.904(4)	1.907(3)
Co(1)−C(15)	1.898(3)	1.903(4)	1.896(3)	1.905(3)	1.900(4)	1.911(3)
Co(1)−C(16)	1.908(3)	1.890(3)	1.905(2)	1.898(3)	1.907(3)	1.903(2)
N(3)−C(11)	1.142(3)	1.151(4)	1.151(3)	1.148(4)	1.146(4)	1.153(3)
C(11)−N(3)−Ln(1)	163.9(2)	174.9(3)	165.11(18)	175.0(2)	165.7(3)	175.2(2)
N(3)−C(11)−Co(1)	173.3(2)	176.1(3)	172.7(2)	176.1(3)	172.4(3)	175.7(2)

the hydrogen bonds between O(1)−N(9) and O(2)−N(10), joins the chains by pairs (Figure 3). These $\pi-\pi$ interaction provide additional stabilization of the crystal structure. Intermolecular stacking distances between centroids of the bpy rings are shown for complexes **1**−**6** and **8**−**13** in Table 5.

Shape Measures. The continuous shape measures (CShM) give an idea of how much a particular structure deviates from an ideal shape. The CShM relative to a polyhedron, *P*, for a set of *N* atoms (in the present case $N = 8$ for a centered polyhedron), characterized by their position vectors Q_i, is defined by eq 1,[11] where P_i is the position vector of the corresponding vertex in the reference polyhedron *P*, and Q_0 the position vector of the geometrical center of the problem structure. The minimum is taken for all possible relative orientations in space, isotropic scaling, and for all possible pairings of the vertexes of the problem and reference polyhedra. All CShM have been calculated with the program SHAPE v1.1a.[12]

$$S_Q(P) = \min \frac{\sum_{i=1}^{N} |Q_i - P_i|^2}{\sum_{i=1}^{N} |Q_i - Q_0|^2} 100 \qquad (1)$$

We have analyzed the CShM of the coordination sphere (eight coordination) of the lanthanide ions of the one-dimensional complexes *trans*-[M(CN)$_4$(μ-CN)$_2$Ln(H$_2$O)$_4$(bpy)]$_n$·4*n*H$_2$O·1.5*n*bpy (**1**−**6**, **8**−**13** and the analogous ones previously reported by us[6a]) relative to several reference eight-vertex polyhedra. The results are summarized in Table S4 (Supporting Information). The coordination polyhedra of the lanthanide ions are close to two ideal polyhedral geometries: square antiprism (SAPR-8) and triangular dodecahedron (DD-8). For a general study of polyhedral eight-vertex structures based on CShM, see Casanova et al.[13]

To compare the measures obtained with respect to DD-8 and SAPR-8, we can make a shape map (a scatterplot of S(DD-8) versus S(SAPR-8), Figure 4). In this plot, we also represent the minimal distortion interconversion path[12] between the two reference polyhedra. This map shows that our structures are very close to the middle of the interconversion path. Therefore, we choose to consider the structure corresponding to the middle of the path (Scheme 1) as a reference polyhedron (that we call *M*). The low CShM values relative to this new reference polyhedron (Table 6), show that it provides the best way to describe the geometry of our experimental structures.

(11) Pinsky, M.; Avnir, D. *Inorg. Chem.* **1998**, *37*, 5575.
(12) Llunell, M.; Casanova, D.; Cirera, J.; Bofill, J. M.; Alemany, P.; Alvarez, S.; Pinsky, M.; Avnir, D. *SHAPE v1.1a* (This program has been developed in the group of Prof. Alvarez at the Universitat de Barcelona and is available from the authors at llunell@qf.ub.es).
(13) Casanova, D.; Llunell, M.; Alemany, P.; Alvarez, S. *Chem. Eur. J.* **2005**, *11*, 147.

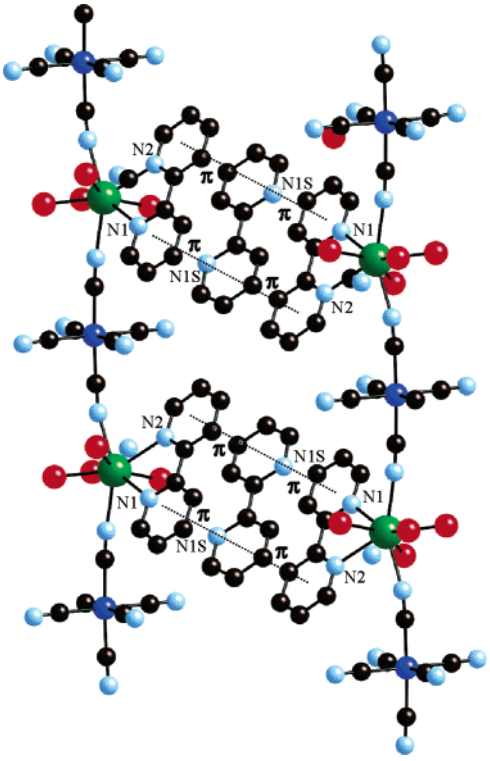

Figure 2. Schematic representation of one set of $\pi-\pi$ interactions of trans-$[Fe(CN)_4(\mu\text{-}CN)_2\ Dy(H_2O)_4(bpy)]_n \cdot 4nH_2O \cdot 1.5n$bpy (**3**). All complexes show similar $\pi-\pi$ interactions.

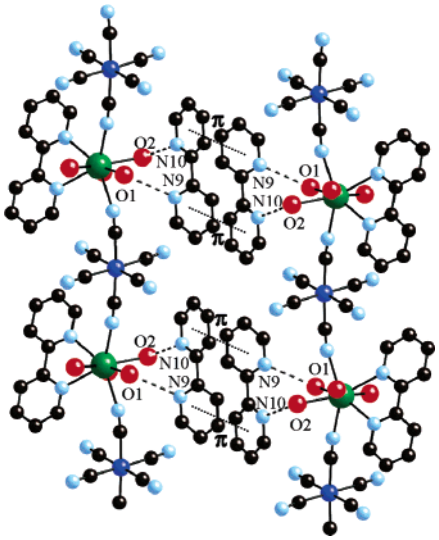

Figure 3. Schematic representation of the other set of $\pi-\pi$ interactions and one set of hydrogen bonds of *trans*-$[Fe(CN)_4(\mu\text{-}CN)_2Dy(H_2O)_4(bpy)]_n \cdot 4nH_2O \cdot 1.5n$bpy (**3**). All complexes show similar interactions.

To understand the deviation of the one-dimensional complexes from the *M* structure, we study the influence of the bite angle (α) of the bpy ligand (Table 6) on the deviation from the ideal geometry, *M*, for which the bite angle is equal to 74.16°. In the complexes under study, the bite angle is smaller than in *M* and the corresponding CShM's are seen to vary in a practically linear way with α (Figure 5). It can be concluded that the bite angle of the bpy ligand is responsible for the deviation of the experimental geometries from the polyhedron in the middle of the interconversion path (*M*) between the dodecahedron and the square antiprism.

The analysis of the experimental data of the octacoordinated dinuclear $[Ln(DMF)_4(H_2O)_3(\mu\text{-}CN)M(CN)_6]\cdot nH_2O$ (M = Fe^{3+} or Co^{3+}) complexes previously prepared by us[3b] together with the analysis of the experimental data retrieved from the Cambridge Structural Database by searching for compounds with a metal atom defined in the database as octacoordinated with the cores $[Ln(bpy)O_4X_2]$ and $[Ln(DMF)_4X_4]$ are shown in the shape map in Figure S1 (Supporting Information). Looking at the shape map for the dinuclear complexes, $[Ln(DMF)_4(H_2O)_3(\mu\text{-}CN)M(CN)_6]\cdot nH_2O$, it is observed that these show a geometry nearest to the square antiprism (SAPR-8). The distortion from this ideal geometry is due to the position of the nitrogen atom of the cyanide bridge coordinated to the lanthanide ion. This distortion for the $[Ce(DMF)_4(H_2O)_3(\mu\text{-}CN)Fe(CN)_6]\cdot nH_2O$ complex is shown, as an example, in Scheme S1, Supporting Information.

Magnetic Studies. Magnetic measurements were performed for the 13 $[LnFe]_n$ and $[LnCo]_n$ complexes. The Ln^{3+} ions used in this research, with the exception of the Lu^{3+}, and the Co^{3+} ion possess a first-order angular momentum, which prevents the use of a spin-only Hamiltonian for isotropic exchange. The approach used in obtaining new insights on the nature of the $Ln^{3+}-Fe^{3+}$ metal ion interactions is the same as that described in Part I of this work. The variable-temperature (2−300 K) measurements for all the complexes have been measured in a field of 8000 G. In all cases, the magnetic susceptibility, χ_M , is per Ln−M unit. The deviation of the magnetic susceptibility of these compounds, with respect to the Curie law, is due entirely to the thermal population of the Ln^{3+} Stark components. In the case of the $[LnFe]_n$ complexes, the anisotropy of the Fe^{3+} ion must also be taken into account.

***trans*-$[Fe(CN)_4(\mu\text{-}CN)_2Eu(H_2O)_4(bpy)]_n \cdot 4nH_2O \cdot 1.5n$bpy (1) and *trans*-$[Co(CN)_4(\mu\text{-}CN)_2Eu(H_2O)_4(bpy)]_n \cdot 4nH_2O \cdot 1.5n$bpy (8).** A plot of χ_MT of $[EuFe]_n$ (**1**) and $[EuCo]_n$ (**8**) compounds is shown at the top of Figure 6, together with χ_MT of $[LuFe]_n$ and $\Delta\chi_MT = \chi_M^{[EuFe]_n}T - \chi_M^{[EuCo]_n}T$. At 300 K the χ_MT value for $[EuCo]_n$ is about 1.60 $cm^3\ mol^{-1}$ K, close to the expected value for one isolated Eu^{3+} ion (the experimental values are in the range 1.44−1.62), and decreases with temperature to 0.01 $cm^3\ mol^{-1}$ K at 2 K (Eu^{3+} has a nonmagnetic ground state, $^7F_0$). At 300 K, the χ_MT value for $[EuFe]_n$ is about 2.20 $cm^3\ mol^{-1}$ K and decreases with the temperature to 0.50 $cm^3\ mol^{-1}$ K at 2 K. $\Delta\chi_MT$ is superimposable with $\chi_M^{[LuFe]_n}T$, indicating that there is negligible interaction between the spin carriers. Furthermore, the experimental magnetization of $[EuFe]_n$ (Figure 6, bottom) is practically superimposable to that of the uncorrelated spin system.

***trans*-$[Fe(CN)_4(\mu\text{-}CN)_2Tb(H_2O)_4(bpy)]_n \cdot 4nH_2O \cdot 1.5n$bpy (2) and *trans*-$[Co(CN)_4(\mu\text{-}CN)_2\ Tb(H_2O)_4(bpy)]_n \cdot 4nH_2O \cdot 1.5n$bpy (9).** A plot of χ_MT of $[TbFe]_n$ (**2**) and $[TbCo]_n$ (**9**) compounds is shown at the top of Figure 7, together with χ_MT of $[LuFe]_n$ and $\Delta\chi_MT$ ($\Delta\chi_MT = \chi_M^{[TbFe]_n}T - \chi_M^{[TbCo]_n}T$). At 300 K the χ_MT value for $[TbCo]_n$ is about

Table 5. Distances between bpy Ring Centroid (Å) for Complexes **1**−**6** and **8**−**13**[a]

	[Eu−Fe]$_n$ (**1**)	[Tb−Fe]$_n$ (**2**)	[Dy−Fe]$_n$ (**3**)	[Ho−Fe]$_n$ (**4**)	[Er−Fe]$_n$ (**5**)	[Tm−Fe]$_n$ (**6**)
Cg(1)−Cg(2)	3.615	3.639	3.629	3.638	3.606	3.649
Cg(2)−Cg(3)	3.642	3.625	3.638	3.638	3.596	3.634
Cg(4)−Cg(5)	3.872	3.861	3.856	3.852	3.843	3.846
	[Eu−Co]$_n$ (**8**)	[Tb−Co]$_n$ (**9**)	[Dy−Co]$_n$ (**10**)	[Ho−Co]$_n$ (**11**)	[Er−Co]$_n$ (**12**)	[Tm−Co]$_n$ (**13**)
Cg(1)−Cg(2)	3.628	3.637	3.646	3.627	3.655	3.635
Cg(2)−Cg(3)	3.633	3.641	3.628	3.652	3.631	3.667
Cg(4)−Cg(5)	3.865	3.857	3.848	3.844	3.841	3.842

[a] Cg(1), ring of N(1); Cg(2), ring of N(1S); Cg(3), ring of N(2); Cg(4), ring of N(9); Cg(5), ring of N(10).

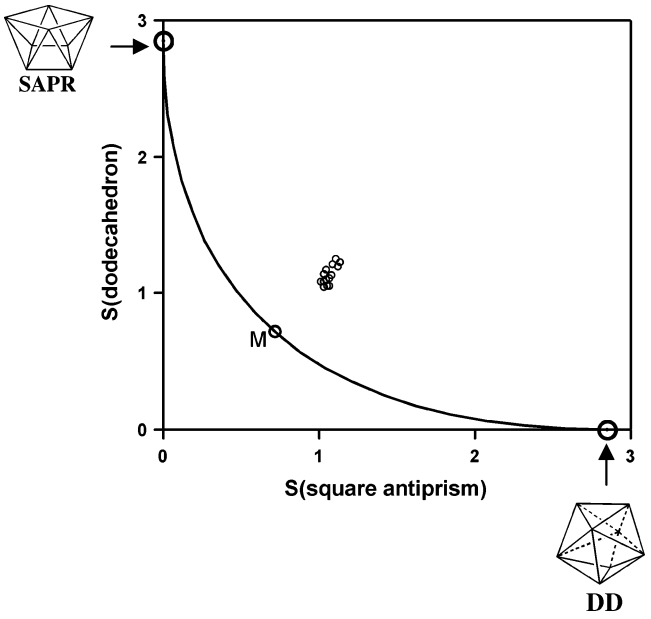

Figure 4. Shape measures of the monodimensional complexes *trans*-$[M(CN)_4(\mu\text{-}CN)_2Ln(H_2O)_4(bpy)]_n \cdot 4nH_2O \cdot 1.5n$bpy plotted in a shape map respect to triangular dodecahedron (DD-8) and square antiprism (SAPR-8). The continuous line represents the minimum distortion interconversion path between these two polyhedra, and the structure at the middle of the path (*M*, see Scheme 1) is represented by a circle.

Scheme 1. Geometry of the Structure in the Middle of the Interconversion Path (*M*) between the Triangular Dodecahedron (DD-8) and the Square Antiprism (SAPR-8)

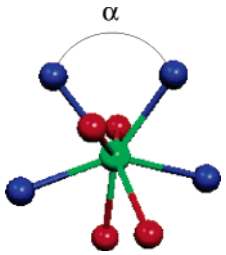

11.83 cm^3 mol^{-1} K, close to the expected value for one isolated Tb^{3+} ion (the calculated value is 11.82 with a *g* value of 3/2), and decreases with temperature to 5.77 cm^3 mol^{-1} K at 2 K. At 300 K, the $\chi_M T$ value for [TbFe]$_n$ is about 12.65 cm^3 mol^{-1} K and decreases with the temperature to 4.31 cm^3 mol^{-1} K at 2 K. From approximately 100 K, $\Delta\chi_M T$ decreases with regard to the $\chi_M^{[LuFe]_n} T$ curve. This profile of the $\Delta\chi_M T$ curve clearly shows that weak antiferromagnetic interactions take place. Furthermore, the experimental magnetization of [TbFe]$_n$ at 2 K (Figure 7, bottom) is lower than that of the uncorrelated spin system, corroborating the antiferromagnetic coupling.

Table 6. Continuous Shape Measures (CShM) with Respect the Polyhedron in the Middle of the Path between DD-9 and SAPR-9 and Values of the Bite Angle of the bpy Ligand for the Experimental Compounds

structure [ML_8]	*S*(*M*)	angle, α (deg)
[SmFe]$_n$[a]	0.50	63.13
[EuFe]$_n$ (**1**)	0.46	63.30
[GdFe]$_n$[a]	0.47	63.77
[TbFe]$_n$ (**2**)	0.42	64.09
[DyFe]$_n$ (**3**)	0.39	64.45
[HoFe]$_n$ (**4**)	0.37	64.85
[ErFe]$_n$ (**5**)	0.35	65.24
[TmFe]$_n$ (**6**)	0.34	65.32
[YbFe]$_n$[a]	0.34	65.77
[EuCo]$_n$ (**8**)	0.43	63.56
[GdCo]$_n$[a]	0.44	64.08
[TbCo]$_n$ (**9**)	0.39	64.29
[DyCo]$_n$ (**10**)	0.38	64.54
[HoCo]$_n$ (**11**)	0.36	64.77
[ErCo]$_n$ (**12**)	0.33	65.29
[TmCo]$_n$ (**13**)	0.31	65.44
[YbCo][a]	0.32	65.82
middle (*M*)	0.00	74.16

[a] Reference 6a.

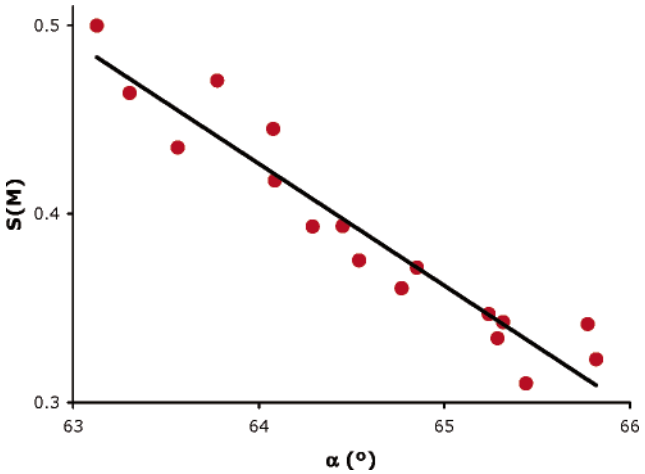

Figure 5. Relationship between the bite angle and the deviation of the structures from the polyhedron (*M*) at the middle of the interconversion path DD-8 /SAPR-8.

***trans*-$[Fe(CN)_4(\mu\text{-}CN)_2Dy(H_2O)_4(bpy)]_n \cdot 4nH_2O \cdot 1.5n$bpy (3) and trans-$[Co(CN)_4(\mu\text{-}CN)_2Dy(H_2O)_4(bpy)]_n \cdot 4nH_2O \cdot 1.5n$bpy (10).** A plot of $\chi_M T$ of [DyFe]$_n$ (**3**) and [DyCo]$_n$ (**10**) compounds, in a field of 8000 G, is shown at the top of Figure 8. At 300 K, the $\chi_M T$ value for [DyCo]$_n$ is about 14.00 cm^3 mol^{-1} K, close to the expected value for one isolated Dy^{3+} ion (the calculate value is 14.17 with a *g* value of 4/3), and decreases with temperature to 9.93 cm^3 mol^{-1} K at 2 K. At 300 K, the $\chi_M T$ value for [DyFe]$_n$ is

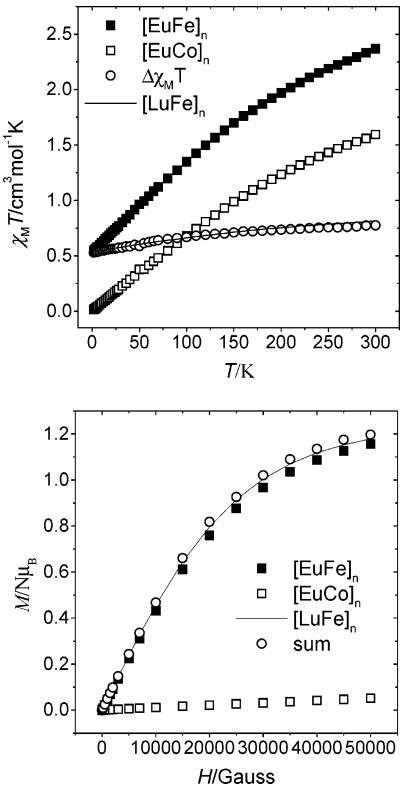

Figure 6. Top: Thermal dependence at 8000 G of $\chi_M T$ of $[EuFe]_n$ (**1**), $[EuCo]_n$ (**8**), $[LuFe]_n$ (**7**), and $\Delta\chi_M T = \chi_M T^{[EuFe]_n} - \chi_M T^{[EuCo]_n}$. Bottom: Magnetization vs H (2 K) of $M^{[EuFe]_n}$, $M^{[EuCo]_n}$, $M^{[LuFe]_n}$, and sum $= M^{[EuCo]_n} + M^{[LuFe]_n}$.

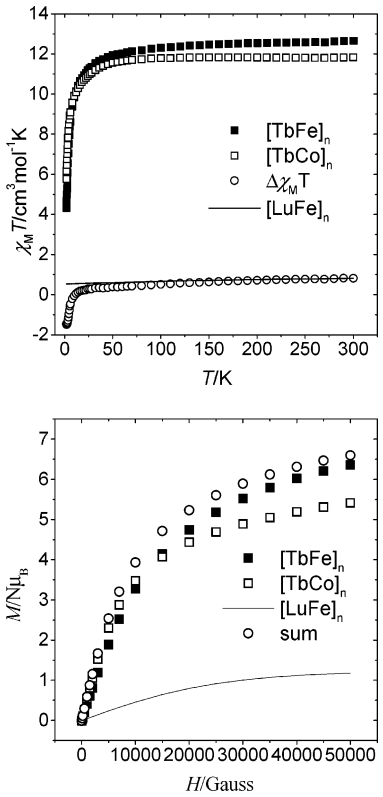

Figure 7. Top: Thermal dependence at 8000 G of $\chi_M T$ of $[TbFe]_n$ (**2**), $[TbCo]_n$ (**9**), $[LuFe]_n$ (**7**), and $\Delta\chi_M T = \chi_M T^{[TbFe]_n} - \chi_M T^{[TbCo]_n}$. Bottom: Magnetization vs H of (2 K) $M^{[TbFe]_n}$, $M^{[TbCo]_n}$, $M^{[LuFe]_n}$, and sum $= M^{[TbCo]_n} + M^{[LuFe]_n}$.

about 14.8 $cm^3\ mol^{-1}$ K and decreases with the temperature to 10.53 $cm^3\ mol^{-1}$ K at 2 K. From approximately 28 K, $\Delta\chi_M T$ decreases with regard to the $\chi_M{}^{[LuFe]_n}T$ curve. This profile of the $\Delta\chi_M T$ curve could indicate that weak antiferromagnetic interaction takes place. Furthermore, the experimental magnetization of $[DyFe]_n$ at 3 K (Figure 8, bottom) is lower than that of the uncorrelated spin system, corroborating the antiferromagnetic coupling.

At low fields, a maximum at 2.5 K in the $\chi_M T$ value is observed. Low-temperature magnetic measurements were carried out to understand this behavior. Susceptibility measurements were carried out at a range of low magnetic fields (Figure 9). When the magnetic field decreased from 400 to 20 G, the maximum of susceptibility increased from 11.36 to 12.63 $cm^3 mol^{-1} K$. The *ac* susceptibility has defined peaks in $\chi''(T)$ signals (Figure 10). The *ac* susceptibility has a small frequency dependence of the peaks, which is perhaps indicative of glassy behavior of the magnetic ordered state.[7d] ZFC-FC measurements at 20 G show a bifurcation point at 2.5 K (Figure 11), which indicates the onset of weak ferromagnetic 3D ordering, possibly due to interchain interactions mediated by hydrogen bonds and/or $\pi-\pi$ stacking. To confirm that the long-range ordering reported in complex $[DyFe]_n$ (**3**) are not due to impurity traces of the 3D compound $Dy[Fe(CN)_6]\cdot 4H_2O$ published by Hulliguer et al.,[8] a comparison of X-ray diffraction patterns was made. In Figures S2 and S3 (Supporting Information), the powder X-ray diffraction patterns of $[DyFe]_n$ (**3**) and $Dy[Fe(CN)_6]\cdot 4H_2O$, in the range $2\theta = 2-60°$ at room temperature, are shown. The superposition of the experimental X-ray diffraction patterns (Figure S4, Supporting Information) indicates that no significant impurity traces of $Dy[Fe(CN)_6]\cdot 4H_2O$ were found. The magnetic measurements are reproducible with different samples coming from different preparations and using the powder pressed in a pellet to prevent preferential crystalline orientation with the magnetic field.

***trans*-$[Fe(CN)_4(\mu\text{-}CN)_2Ho(H_2O)_4(bpy)]_n\cdot 4nH_2O\cdot 1.5n$bpy (4) and *trans*-$[Co(CN)_4(\mu\text{-}CN)_2Ho(H_2O)_4(bpy)]_n\cdot 4nH_2O\cdot 1.5n$bpy (11).** A plot of $\chi_M T$ of $[HoFe]_n$ (**4**) and $[HoCo]_n$ (**11**) compounds is shown at the top of Figure S5 (Supporting Information), together with $\chi_M T$ of $[LuFe]_n$ and $\Delta\chi_M T = \chi_M{}^{[HoFe]_n}T - \chi_M{}^{[HoCo]_n}T$. At 300 K, the $\chi_M T$ value for $[HoCo]_n$ is about 14.11 $cm^3\ mol^{-1}$ K, close to the expected value for one isolated Ho^{3+} ion (the calculated value is 14.07 with a g value of 5/4); it decreases with temperature to 2.85 $cm^3\ mol^{-1}$ K at 2 K. At 300 K, the $\chi_M T$ value for $[HoFe]_n$ is about 14.84 $cm^3\ mol^{-1}$ K and decreases with the temperature to 3.19 $cm^3\ mol^{-1}$ K at 2 K. $\Delta\chi_M T$ is practically superimposable with $\chi_M{}^{[LuFe]_n}T$, indicating that there is negligible interaction between the spin carriers. Furthermore, the experimental magnetization of $[HoFe]_n$ (Figure S5, bottom, Supporting Information) is practically superimposable with that of the uncorrelated spin system.

***trans*-$[Fe(CN)_4(\mu\text{-}CN)_2Er(H_2O)_4(bpy)]_n\cdot 4nH_2O\cdot 1.5n$bpy (5) and trans-$[Co(CN)_4(\mu\text{-}CN)_2Er(H_2O)_4(bpy)]_n\cdot 4nH_2O\cdot 1.5n$bpy (12).** A plot of $\chi_M T$ of $[ErFe]_n$ (**5**) and $[ErCo]_n$ (**12**) is shown at the top of Figure S6 (Supporting Information), together with $\chi_M T$ of $[LuFe]_n$ and $\Delta\chi_M T =$

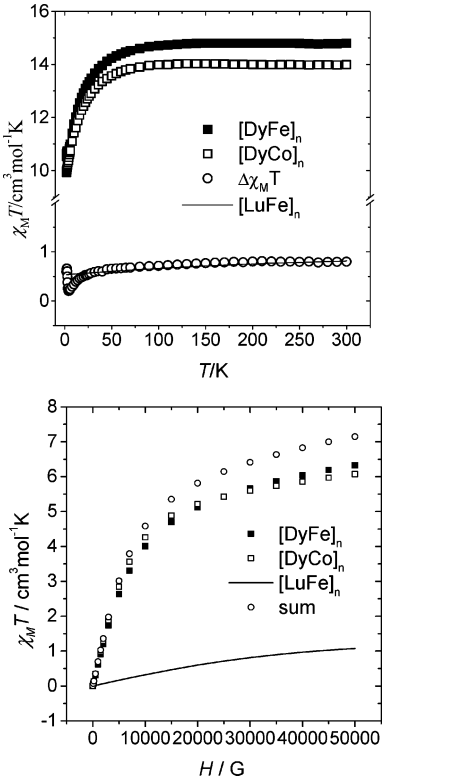

Figure 8. Top: Thermal dependence at 8000 G of $\chi_M T$ of [DyFe]$_n$ (**3**), [DyCo]$_n$ (**10**), [LuFe]$_n$ (**7**), and $\Delta\chi_M T = \chi_M T^{[DyFe]_n} - \chi_M T^{[DyCo]_n}$. Bottom: Magnetization vs H (3 K) of $M^{[DyFe]_n}$, $M^{[DyCo]_n}$, $M^{[LuFe]_n}$, and sum = $M^{[DyCo]_n} + M^{[LuFe]_n}$.

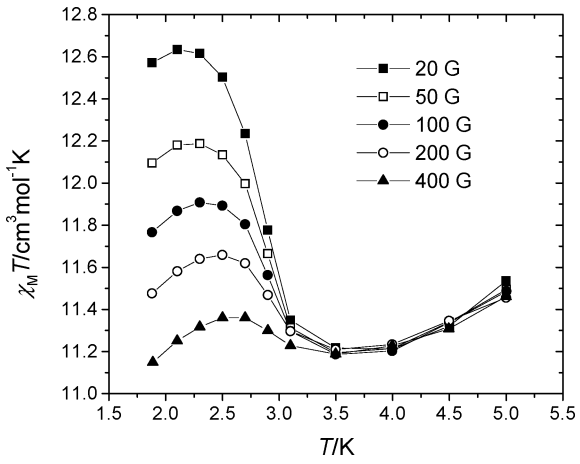

Figure 9. Thermal dependence at different low fields (from 400 to 20 G) of $\chi_M T$ for [DyFe]$_n$ (**3**).

$\chi_M^{[ErFe]_n}T - \chi_M^{[ErCo]_n}T$. At 300 K, the $\chi_M T$ value for [ErCo]$_n$ is about 11.40 cm^3 mol^{-1} K, close to the expected value for one isolated Er^{3+} ion (the calculated value is 11.48 with a g value of 6/5); it decreases with temperature to 8.12 cm^3 mol^{-1} K at 2 K. At 300 K, the $\chi_M T$ value for [ErFe]$_n$ is about 12.23 cm^3 mol^{-1} K and decreases with the temperature to 8.72 cm^3 mol^{-1} K at 2 K. $\Delta\chi_M T$ is practically superimposable with $\chi_M^{[LuFe]_n}T$, indicating that there is negligible interaction between the spin carriers. Furthermore, the experimental magnetization of [ErFe]$_n$ (Figure S6, bottom, Supporting Information) is practically superimposable with that of the uncorrelated spin system.

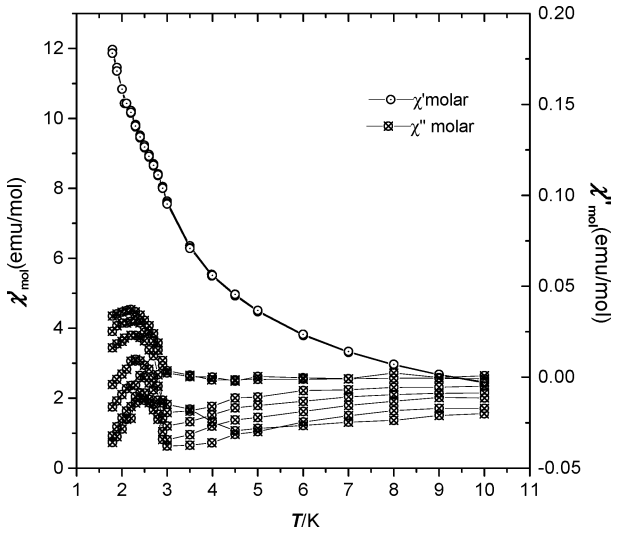

Figure 10. Plot of the in-phase (χ') and out-of-phase (χ'') components of the *ac* susceptibility of [DyFe]$_n$ (**3**), at 1500, 1250, 1000, 750, 500, 100, and 50 Hz.

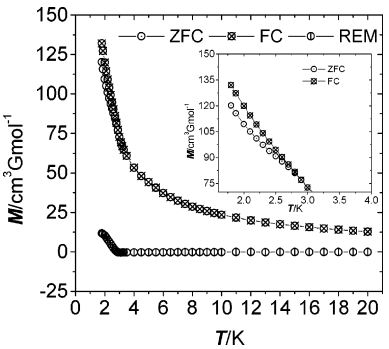

Figure 11. Plot of the zero-field-cooled (ZFC), field cooled (FC), and remnant magnetization of [DyFe]$_n$ (**3**) measured in a 20 G applied field.

***trans*-[Fe(CN)$_4$(μ-CN)$_2$Tm(H$_2$O)$_4$(bpy)]$_n$·4*n*H$_2$O·1.5*n*bpy (6) and *trans*-[Co(CN)$_4$(μ-CN)$_2$Tm(H$_2$O)$_4$(bpy)]$_n$·4*n*H$_2$O·1.5*n*bpy (13).** A plot of $\chi_M T$ of [TmFe]$_n$ (**6**) and [TmCo]$_n$ (**13**) is shown at the top of Figure S7 (Supporting Information), together with $\chi_M T$ of [LuFe]$_n$ and $\Delta\chi_M T = \chi_M^{[TmFe]_n}T - \chi_M^{[TmCo]_n}T$. At 300 K, the $\chi_M T$ value for [TmCo]$_n$ is about 7.05 cm^3 mol^{-1} K, close to the expected value for one isolated Tm^{3+} ion (the calculated value is 7.15 with a g value of 7/6), and decreases with temperature to 5.86 cm^3 mol^{-1} K at 2 K. At 300 K, the $\chi_M T$ value for [TmFe]$_n$ is about 7.80 cm^3 mol^{-1} K and decreases with the temperature to 6.33 cm^3 mol^{-1} K at 2 K. $\Delta\chi_M T$ is practically superimposable with $\chi_M^{[LuFe]_n}T$, indicating that there is negligible interaction between the spin carriers. Furthermore, the experimental magnetization of [TmFe]$_n$ (Figure S7, bottom, Supporting Information) is practically superimposable with that of the uncorrelated spin system.

Conclusions

Thirteen [LnFe]$_n$ and [LnCo]$_n$ monodimensional systems have been characterized and magnetically studied. When comparing the structural results of Part I and Part II of this work and the results of the isostructural one-dimensional complexes previously reported by us,[6a] an interesting feature appears. The early lanthanide ions of the series give trinuclear

complexes in which the coordination number is nine (four nitrogen atoms of two bpy molecules, four oxygen atoms of four coordinated water molecules, and one nitrogen atom from one cyanide bridge ligand). Completing the series with the other lanthanide ions, one-dimensional structures were found in which the coordination number of the lanthanide ions is eight (two nitrogen atoms of one bpy molecule, four oxygen atoms of four coordinated water molecules, and two nitrogen atoms from two cyanide bridge ligands). Comparing the two geometries, the eight-coordination was achieved by losing a bpy molecule and adding a new cyanide-bridged ligand, which is the one responsible for the one-dimensional structure. In the dinuclear complexes published by us using DMF as blocking ligand (monodentate), instead of bpy (bidentate), no changes along the full lanthanide series were found, so the bpy ligand plays an important role in building the structure. Throughout the lanthanide series, a contraction of the radium value is manifest, so a diminution in the coordination number may be justified. When the building block is $[Fe(CN)_6]^{3-}$, the Sm^{3+} is the limit of the trinuclear complexes; however, when the building block is $[Co(CN)_6]^{3-}$, the Nd^{3+} is the new limit of the trinuclear complexes. Thus, the small volume of the $[Co(CN)_6]^{3-}$ with regard to $[Fe(CN)_6]^{3-}$ can also play a role in building the structure. In conclusion, in these structural changes, neither the lanthanide ion nor the building block $[M(CN)_6]^{3-}$ nor the bpy blocking ligand are innocent. The coordination polyhedron of the lanthanide ions is in the middle of the minimal distortion path between the two ideal geometries (square antiprism and triangular dodecahedron); the bite angle of the bpy ligand is responsible for the deviation of the minimal distortion path between the two ideal geometries.

Most of the 3d−4f complexes that show long-range magnetic ordering involve the Sm^{3+} ion. The replacement of the Sm^{3+} ion by another lanthanide ion usually gives rise to isostructural compounds that lose all three-dimensional magnetic properties. In the systems that are the object of this work, weak long-range magnetic ordering was observed in the $[DyFe]_n$ (**3**) compound with a T_c equal to 2.5 K. To the best of our knowledge, in f−d systems involving Dy^{3+}, only one three-dimensional compound of formula $Dy[Fe(CN)_6]\cdot 4H_2O$ with T_c equal to 2.8 K[8] and a spin-ladder molecular complex abbreviated by Dy_2Cu_3 with T_c equal to 0.75 K[14] are found in the literature. Complex **3** is thus the second d-Dy complex that shows long-range magnetic order and that is not three-dimensional.

Acknowledgment. This work was financially supported by Spanish Government (Grant No. BQU2003-00539).

Supporting Information Available: Additional tables, figures and crystallographic data in cif format. This material is available free of charge via the Internet at http://pubs.acs.org.

IC050650+

(14) Evangelisti, M.; Kahn, M. L.; Bartalomé, J.; Jongh, L. J.; Meyers, C.; Leandri, J.; Leroyer, Y.; Mathonière, C. *Phys. Rev. B* **2003**, *68*, 184405.